J. T. K. L.
JURNAL TEKNIK KIMIA DAN LINGKUNGAN

*J. Tek. Kim. Ling. 2026, 10 (1), 34-45*
p-ISSN : 2579-8537, e-ISSN : 2579-9746
http://jurnal.polinema.ac.id/index.php/jtkl
DOI: http://dx.doi.org/10.33795/jtkl.v10i1.8871

# Isotherm and Kinetic Adsorption of Nitrogen–Doped Carbon for Remazol Brilliant Blue R Dye

**Susanto Susanto[1,*], Handoko Desta Priadi[1], Mahhathir Muhammad[1], Agus Jalaluddin[1], Ricka Prasdiantika[2]**

[1]Department of Chemical Engineering, Politeknik Negeri Malang, Jl. Soekarno Hatta No. 9, Malang 65141, Indonesia
[2]Department of Pharmaceutical and Food Analysis, Politeknik Kesehatan Kemenkes Surakarta, Jl. Letjend Sutoyo, Surakarta 57127, Indonesia

## ABSTRACT

Industrial textile effluents containing Remazol Brilliant Blue R (RBBR) represent a significant environmental challenge due to their persistent nature and resistance to conventional biological treatment methods. This research explores the development of nitrogen-enriched carbon materials derived from palm oil empty fruit bunch (PEFB) cellulose as an effective adsorbent for RBBR elimination from contaminated water systems. The synthesized material was produced through thermal treatment at 700°C, enabling the formation of pyridinic nitrogen groups that improve surface alkalinity and create electron-rich active sites. Material characterization employed XRD, FTIR, and SEM-EDS techniques to evaluate structural and chemical properties. Laboratory-scale adsorption studies examined the influence of starting dye concentrations (100-500 mg/L) and reaction duration (10-120 minutes). Results demonstrated optimal fitting with the Freundlich isotherm model ($q_m$ = 434.78 mg/g) and pseudo-second-order kinetics, suggesting heterogeneous multilayer adsorption dominated by chemical bonding mechanisms. The proposed interaction mechanism involves electrostatic attraction between RBBR sulfonate functionalities and protonated pyridinic nitrogen sites under pH 6 conditions.

**Keywords:** adsorption, nitrogen–doped carbon, oil palm empty fruit bunch, Remazol Brilliant Blue R, wastewater treatment.

## 1. INTRODUCTION

Industrial sectors including leather processing, food manufacturing, cosmetics production, paper mills, textile dyeing, rubber manufacturing, and printing operations generate substantial volumes of dye-containing wastewater. Approximately half of all colorants utilized in textile manufacturing processes ultimately appear in discharged effluents [1]. These textile wastewaters rank among the most hazardous environmental contaminants due to their large discharge volumes and complex chemical composition, reflecting significant dye losses during coloration processes [2]. Among various colorant pollutants found in industrial discharges, RBBR stands out as a particularly concerning contaminant. Its excellent water solubility, high reactivity, considerable toxicity, and tendency toward environmental persistence make RBBR a frequently detected pollutant in industrial wastewater streams [3]. The non-biodegradable and resistant characteristics of RBBR create it a harmful organic pollutant [4]. The majority of azo dyes have been identified as the primary contributors to cancer of the bladder in humans, hepatic sarcomas, and chromosomal abnormalities in mammalian cells [5]. Consequently, it is imperative that the effluents containing the hazardous RBBR dye undergo thorough treatment, ensuring that their concentrations are diminished to a permissible level prior to being released into the river. Therefore, comprehensive treatment of RBBR-containing effluents becomes essential to reduce concentrations to acceptable levels before environmental discharge. RBBR removal poses significant technical

[*]Corresponding author:
E-mail: susanto.s@polinema.ac.id (Susanto Susanto)
How to cite: Susanto, et al., Jurnal Teknik Kimia dan Lingkungan 10 (2026) 34–46.

Submitted : September 26, 2025
Revised : December 01, 2025
Accepted : December 25, 2025

challenges due to its stable complex aromatic structure. Direct wastewater discharge often leads to bioaccumulation in human systems and aquatic environments [6].

Various treatment technologies have been developed for hazardous compound removal from wastewater, including membrane separation, electrochemical processes, coagulation-flocculation, ozone treatment, biological degradation, advanced oxidation, and photocatalytic degradation [7]. nevertheless, these methods exhibit numerous disadvantages, including substantial capital and operational expenses, the intricacy of treatment procedures, challenges associated with sludge disposal, and the requirement for chemicals that may subsequently contaminate the water [8]. Adsorption processes offer significant advantages for removing toxic pollutants from textile and dyeing industry effluents, including economic feasibility, simple and flexible operation, ease of implementation, adsorbent recovery potential, and tolerance to inhibitory substances [9].

Activated carbon materials are recognized for their exceptional specific surface areas, porous structures, and thermal stability. These properties make them suitable for diverse applications including pollutant and odor removal from liquid and gaseous phases, medical applications, catalytic processes, gas storage systems, electrode materials for energy devices, and organic contaminant elimination from drinking water and wastewater [10]. Adsorption on active carbon is an effective method for dye removal from wastewater, characterized by its capacity to adsorb a wide array of contaminants, rapid adsorption kinetics, straightforward design, and economical price [11].

Indonesia possesses substantial potential for PEFB utilization due to extensive palm oil production. Indonesian Central Bureau of Statistics reports indicate crude palm oil production in East Kalimantan reached 16,717,254 tons in 2021 [12]. With approximately 23% of fresh fruit bunches consisting of empty bunches [13], this corresponds to an estimated 3.84 million tons of PEFB generated. This biomass creates waste management challenges including disposal difficulties, landfill contamination, and groundwater pollution from leachate. Additionally, the combustion of biomass results in the release of hazardous smoke and poisonous substances, including dioxins. Consequently, research on the efficient exploitation and recovery of PEFB has become an urgent and major topic [14].

This study aimed to synthesis nitrogen-doped carbon from cellulose pulp obtained from PEFB, leveraging its superior physico–chemical properties and abundant pyridinic N functionalities for the efficient removal of the anionic dye RBBR. Pyrolysis at 700 °C facilitated the incorporation of pyridinic N groups [15], which enhance surface basicity and provide electron donating active sites analogous to amine functionalities. Although nitrogen–doped carbon materials have shown promising potential, their application in RBBR adsorption remains scarcely explored. Several characterization techniques were employed for explaining the structural and chemical features of nitrogen-doped carbon. Additionally, key parameters including initial concentration and contact duration were investigated through batch experiments. Adsorption equilibrium and kinetic analysis were conducted, and a mechanistic proposal for the adsorption process was presented.

## 2. RESEARCH METHODS

### 2.1. Material

Raw materials included palm empty fruit bunches (PEFB with 49% cellulose), ammonia solution ($NH_4OH$ 25%), urea ($(NH_2)_2CO$), ethanol ($C_2H_5OH$ 99.9%), hydrogen peroxide ($H_2O_2$ 50%), sodium hydroxide (NaOH), Remazol Brilliant Blue R (RBBR), potassium dihydrogen phosphate ($KH_2PO_4$), and Batik waste with RBBR dye.

### 2.2. Synthesis of Adsorbent Material

PEFB were initially processed and sieved to get a powder with a particle size of 150 mesh. The powder followed alkaline digestion

using a 17.5% NaOH solution (20 mL per gram of PEFB) at 90°C for 2 hours. Following treatment, the resulting pulp was filtered and thoroughly washed with demineralized water. Bleaching procedures involved treating pulp with 3% hydrogen peroxide at pH 9 and 90°C for one hour. The bleached cellulose pulp was subsequently dissolved in a cross-linking solvent system containing 1 g NaOH, 7.8 mL $NH_4OH$, 4 g urea, and 10 mL demineralized water. The solution underwent freezing at -12°C for 24 hours to promote gel formation. The gel was then thawed at ambient temperature and separated from residual liquid. Coagulation occurred using 96% ethanol for 24 hours, followed by solvent exchange with demineralized water. Subsequently, samples were frozen at -20°C for 24 hours, then freeze-dried at -40°C and 20 Pa for an additional 24 hours using freeze-drying equipment. The cellulose aerogel underwent carbonization in nitrogen atmosphere at 700°C for 2 hours to produce nitrogen-doped carbon aerogel.

### 2.3. Adsorption Batch Studies

Adsorption experiments were conducted in batch mode to assess nitrogen-doped carbon effectiveness for RBBR elimination from aqueous solutions. Each experiment involved adding 10 mg adsorbent to 20 mL RBBR solution in sampling containers and agitating at 200 rpm using an orbital shaker. To examine initial dye concentration effects, RBBR solutions of 100, 200, 300, 400, and 500 mg/L were prepared at constant pH 6, with fixed contact time of 60 minutes. Adsorption was done at pH 6, because based on the literature study of adsorption RBBR by carbon-based materials optimum at the pH [4].

The optimal concentration from this phase was used for kinetic studies. In kinetic experiments, contact time varied at 10, 20, 30, 40, 50, 60, 90, and 120 minutes while maintaining pH and agitation speed. After adsorption, adsorbent separation occurred through filtration using Whatman No. 42 filter paper. Filtrates were collected in sampling bottles, and residual RBBR concentrations were measured using UV-Visible spectrophotometer (Hitachi U-2900) at peak wavelength 595 nm. A calibration curve for absorbance was established using standard dye solutions as reference for concentration determination.

Dye removal percentage and adsorbent efficiency (%A) calculations used the following expression:

$$\%A = \frac{(C_0 - C_e)}{C_0} \times 100 \quad (1)$$

Equilibrium adsorption capacity (mg/g) of RBBR ($q_e$) was determined using:

$$q_e = \frac{(C_0 - C_e)\ V}{m} \quad (2)$$

where $C_0$ represents initial RBBR solution concentration (mg/L), $C_e$ represents equilibrium RBBR concentration (mg/L), $V$ represents solution volume (L), and $m$ represents adsorbent mass (g).

### 2.4. Characterization Analysis of Nitrogen–Doped Carbon

The structural and surface properties of the adsorbent were characterized. To identify the functional groups on the adsorbent surface, Fourier–transform infrared spectroscopy (FTIR; Thermo Scientific Nicolet iS10) was applied, with the wavenumber range of 4000–400 $cm^{-1}$. The morphology and elemental composition were analyzed using scanning electron microscopy with energy-dispersive X-ray spectroscopy at energy of 15 kV and resolution at 133.6 eV (SEM–EDS; Hitachi FlexSEM 1000). The material's crystalline phase and structural order have been identified using X-ray diffraction (XRD; PANalytical X'pert Pro) within the 2θ range of 5–80°.

### 2.5. Adsorption Isotherms

Langmuir and Freundlich were the two linear classic isotherm models employed in this investigation. The Langmuir isotherm model is valid for monolayer adsorption and implies that interactions between sorbent molecules

are insignificant. Langmuir isotherm is indicated by as:

$$\frac{C_e}{q_e} = \frac{C_e}{q_m} + \frac{1}{K_L q_m} \quad (3)$$

The Freundlich isotherm is an empirical model that describes the adsorption process that takes place on a heterogeneous surface in a multilayer system. The formula that predicts this model is as follows:

$$\log q_e = \log C_e \frac{1}{n} + \log K_F \quad (4)$$

where $C_e$ is the concentration of dyes at equilibrium (mg/L), $q_m$ is the maximum adsorption capacity (mg/g), $q_e$ is the quantity of dyes absorbed at time, $K_L$ is the Langmuir rate constant, then $K_F$ is constants of Freundlich and $n$ is the rate constants of Freundlich.

### 2.6. Adsorption Kinetics

The pseudo-first-order, pseudo-second-order, and intra-particle diffusion models were employed to analyze the RBBR adsorption data, as detailed below. Lagergren proposed the pseudo-first-order kinetic model for the adsorption of solid/liquid systems, and its formula is as follows:

$$\log (q_e - q_t) = \log q_e - \frac{k_1}{2.303} t \quad (5)$$

where $q_t$ (mg/g) and $q_e$ (mg/g) represent dye amounts adsorbed at time $t$ (min) and equilibrium, respectively, and $k_1$ (1/min) represents pseudo-first-order adsorption rate constant. $k_1$ calculation uses log ($q_e$ - $q_t$) versus $t$ plotting.

The pseudo-second-order kinetic model in linear form can be expressed as:

$$\frac{1}{q_t} = \frac{C_e}{k_2 {q_e}^2} + \frac{1}{q_e} \quad (6)$$

where $k_2$ (g/(mg·min)) represents pseudo-second-order adsorption rate constant, determined by linear plots of $t/q_t$ versus $t$.

## 3. RESULTS AND DISCUSSION

### 3.1. Characteristics of a N-Doped Carbon Adsorbent

XRD analysis (Figure 1) revealed a significant structural transformation of OPEFB during pyrolysis and nitrogen modification. The raw PEFB pulp exhibited two sharp diffraction peaks at 2θ = 15.8° and 22.13°, corresponding to [110] and [200] crystallographic planes characteristic of crystalline cellulose [16]. These peaks indicate the dominance of native crystalline domains in the biomass prior to thermal treatment. After pyrolysis, the XRD pattern changed markedly to broad, low–intensity peaks centered at 2θ = 22.82° [002] and 41.92° [101], indicative of decreased crystallinity and the formation of amorphous carbon [17]. Such peak broadening reflects a loss of long–range atomic order due to the thermal degradation of the cellulose polymer chains and for biomass pyrolyzed at 600–800°C [15] .

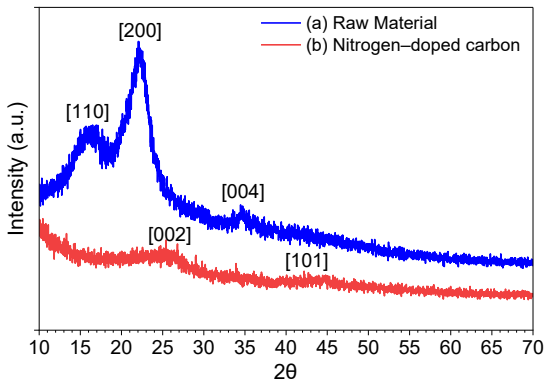


**Figure 1.** XRD patterns of (a) raw PEFB cellulose pulp and (b) nitrogen–doped carbon derived from PEFB.

These structural changes were corroborated by FTIR analysis (Figure 2), which demonstrated the transformation of functional groups upon pyrolysis and nitrogen doping. The origin PEFB spectra displayed characteristic cellulose bands, including a broad –OH stretching vibration at 3334–3340 $cm^{-1}$, aliphatic C–H stretching at 2895 $cm^{-1}$, aromatic C–C vibrations at 1423–1455 $cm^{-1}$, and C–O stretching at 1031 $cm^{-1}$ [18]. After pyrolysis, most of these cellulose–specific bands were diminished or absent,

indicating the decomposition of native organic functionalities. A broad band at 3301 $cm^{-1}$ persisted, assigned to overlapping –OH and –NH stretching, suggesting partial retention of hydroxyl groups and successful incorporation of amine functionalities from nitrogen doping. The presence of absorption bands at 1724 $cm^{-1}$ (C=O), 1649 $cm^{-1}$ (aromatic C=N), and in the range of 1550–1650 $cm^{-1}$ (pyridinic N) indicated the existence of nitrogen-containing aromatic carbon frameworks [15,19].

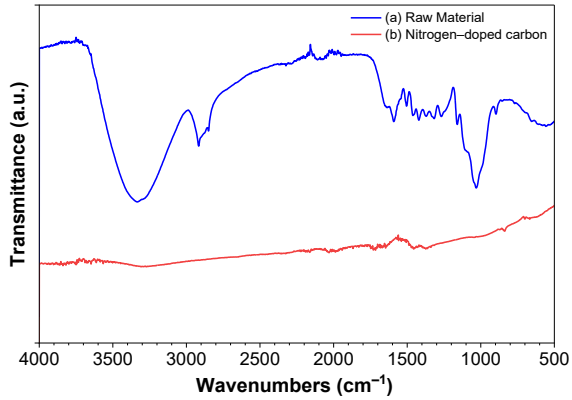


**Figure 2.** FTIR spectra (a) raw PEFB cellulose pulp and (b) nitrogen–doped carbon.

Furthermore, peaks at 1568-1593 $cm^{-1}$ (C=N stretching), 1425 $cm^{-1}$ (C=C stretching), and 880 $cm^{-1}$ (aromatic C–H bending) indicated pyridinic N, while bands at 1080 $cm^{-1}$ (C–N stretching), 1607 $cm^{-1}$ (N–H bending), and 3359 $cm^{-1}$ (N–H stretching) were attributed to pyrrolic nitrogen [20]. These nitrogen functionalities are known to introduce basic active sites, enhancing electrostatic interactions with anionic pollutants.

The porous structure of the nitrogen-doped carbon based on SEM (Figure 3a). EDS analysis (Figure 3.b) further supported these findings, showing that the adsorbent surface was composed predominantly of carbon (56.76 at.%), followed by oxygen (32.73 at.%) and nitrogen (10.51 at.%). The high carbon content confirms the successful formation of a carbonaceous matrix through biomass pyrolysis. In contrast, the significant oxygen content suggests the retention of polar functional groups, such as hydroxyl and carbonyl, which contribute to surface hydrophilicity and reactivity. The relatively high nitrogen content is consistent with the FTIR results, confirming successful nitrogen doping and the presence of a pyridinic N, which is expected to enhance adsorption performance toward anionic dyes.

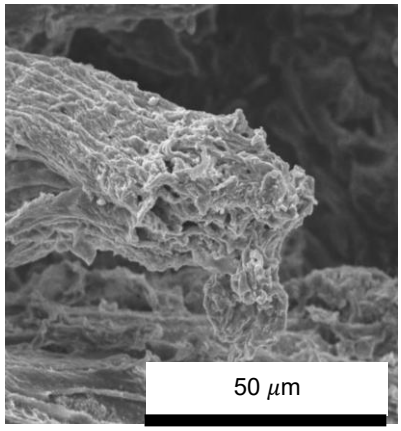


(a)

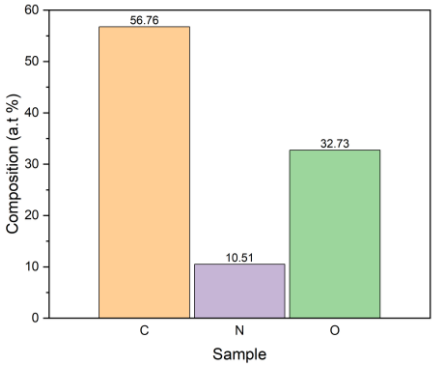


(b)

**Figure 3.** (a) Surface morphology on N-doped carbons based on SEM and (b) atomic composition of nitrogen–doped carbon based on EDS analysis.

### 3.2. Adsorption Batch Studies

#### 3.2.1. Effect of Initial Concentration

Based on Figure 4, results demonstrated contrasting relationships between adsorption capacity ($q_e$) and removal percentage as initial RBBR concentration increased. Increasing initial concentration from 100 to 500 mg/L resulted in significant sorbed RBBR increases from 66.451 mg/g to 225.806 mg/g. At higher concentrations, greater mass transfer driving forces facilitate overcoming mass transfer resistance by RBBR molecules [21]. Conversely, the

adsorption percentage decreased. This is likely due to the aggregation of RBBR molecules at high concentrations [22]. Increasing initial dye concentration causes removal efficiency decreases, potentially due to adsorbent surface adsorption site saturation [23,24]. Therefore, an 100 mg/L initial concentration resulted in the highest adsorption percentage.

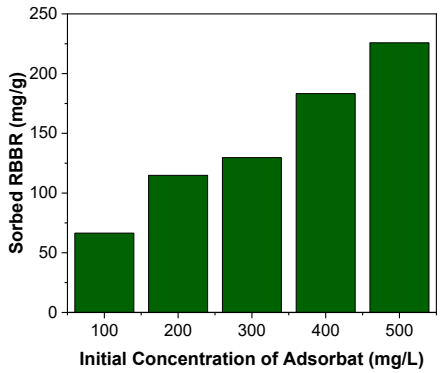


(a)

(b)

**Figure 4.** Effect of initial RBBR concentration on (a) sorbed RBBR and (b) RBBR removal efficiency by nitrogen–doped carbon.

### 3.2.2. Effect of Adsorption Contact Time

Based on Figure 5, maximum sorbed RBBR of 57.742 mg/g was achieved at 50 minutes contact time. This indicates rapid initial adsorption phases due to abundant available active sites. After 50 min, the adsorption rate slowed down as the system approached equilibrium, reaching a saturation point caused by the decrease in available active sites and repulsion between adsorbed and unadsorbed molecules. Interestingly, a decrease in adsorption capacity was observed after the 50 min mark, specifically at 60 and 90 min. The decrease of sorbed RBBR is assumed to occur in the desorption process, a process in which adsorbate molecules are released from the surface of the adsorbent [25]. However, the sorbed RBBR increased again at 120 min. This subsequent rise can be explained by the re–exposure of previously blocked or inaccessible active sites, allowing for renewed adsorption. These fluctuations highlight that the adsorption process is not always linear but is a dynamic phenomenon influenced by simultaneous desorption–readsorption dynamics [26]. At the times, the dye begins to jostle to enter the pores. As in Figure 3.a, Nitrogen doped carbon has a porous structure. The porous structure of the nitrogen-doped carbon (Figure 3.a) allows dye molecules to undergo multi-step diffusion, where molecules may temporarily desorb from surface sites before penetrating deeper into the internal pore network.

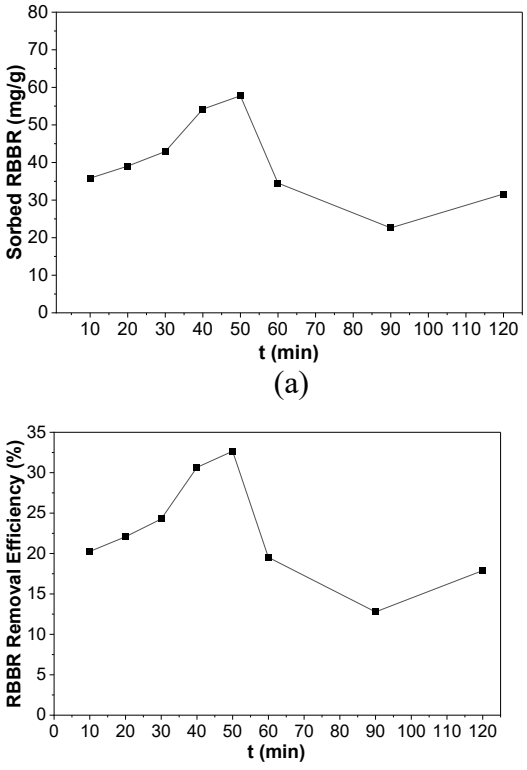


(a)

(b)

**Figure 5**. Effect of contact time on (a) sorbed RBBR and (b) removal efficiency by nitrogen–doped carbon.

### 3.3. Adsorption Isotherm

Based on Figure 6 and Table 1, the adsorption equilibrium data for RBBR onto nitrogen–doped carbon fitted the Freundlich model ($R^2$ = 0.9824, $q_m$ = 434.78 mg/g) better than the Langmuir model ($R^2$ = 0.8208). The significant correlation shows that the adsorption process occurred on a heterogeneous surface characterized by a non-uniform energy distribution, corresponding with the concepts of the Freundlich isotherm [27]. The model also supports the possibility of multilayer adsorption, where molecules are not restricted to a monolayer but can occupy multiple adsorption layers depending on the available active sites and their binding energies. In heterogeneous porous carbons, such as the synthesized nitrogen–doped carbon, adsorption is influenced by the coexistence of micro–, meso–, and macropores, each offering different adsorption energies [28,29].

The high adsorption capacity observed reflects the synergistic effect of the aerogel's hierarchical porosity and its nitrogen–enriched surface chemistry. Similar trends have been reported for nitrogen–doped porous carbons, where multilayer adsorption is facilitated by both surface heterogeneity and intrapore diffusion [30]. In this study, the Freundlich model's good fit suggests that pore penetration plays a significant role alongside surface adsorption, making the process more efficient. Overall, the adsorption mechanism of RBBR onto the nitrogen–doped carbon can be described as a complex, multi–step process involving heterogeneous surface sites, multilayer coverage, and diffusion within interconnected pores.

**Table 1.** Model constants for adsorption isotherms of RBBR onto nitrogen-doped carbon.

| Isotherm models | Parameters | RBBR |
|---|---|---|
| Langmuir | $q_m(mg\ g^{-1})$ | 434.783 |
| | $K_L(mg\ L^{-1})$ | 0.00255 |
| | $R^2$ | 0.8208 |
| Freundlich | $n$ | 1.4945 |
| | $K_F(mg\ g^{-1})$ | 4.1106 |
| | $R^2$ | 0.9824 |

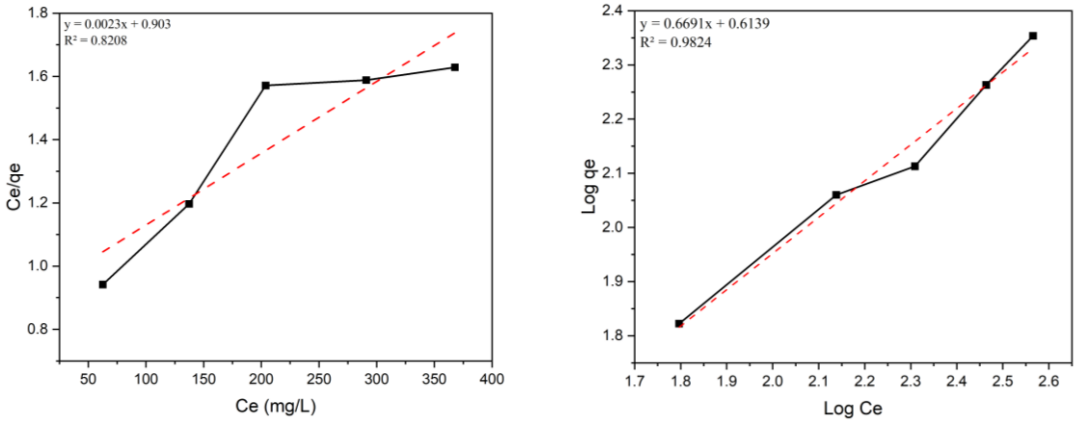


(a) (b)

**Figure 6.** Isotherm models of adsorption RBBR onto nitrogen–doped carbon : (a) Langmuir dan (b) Freundlich.

### 3.4. Adsorption Kinetics

Kinetic modeling explains the mechanism, specifically the potential rate-controlling stage in the dye adsorption process. This research employed pseudo-first-order and pseudo-second-order models to investigate reactive dye adsorption kinetics. Based on Figure 7 and Table 2, linear regression analysis of kinetic data indicated RBBR adsorption on nitrogen-doped carbon is best described by pseudo-second-order kinetic models, exhibiting determination coefficients ($R^2$) of 0.9247. In contrast, pseudo-first-order models showed weaker correlations with considerably lower $R^2$ values of 0.7762. Furthermore, calculated equilibrium adsorption capacities ($q_e$) obtained from pseudo-second-order models at various initial dye concentrations closely matched experimental $q_e$ values.

This significant acceptance offers additional verification that the control of rate mechanism throughout the adsorption process is likely determined by chemical interactions, confirming that chemisorption predominantly affects the adsorption of RBBR onto the modified adsorbent [31].

**Table 2.** Adsorption kinetics model constants for adsorption of RBBR onto nitrogen–doped carbon.

| Kinetics models | Parameters | RBBR |
|---|---|---|
| Pseudo–first order model | $q_e(mg\ g^{-1})$ | 50.3733 |
| | $k_1(min^{-1})$ | 0.05688 |
| | $R^2$ | 0.7762 |
| Pseudo–second order model | $q_e(mg\ g^{-1})$ | 64.1026 |
| | $k_2(gmg^{-1}min^{-1})$ | 0.00146 |
| | $R^2$ | 0.9247 |

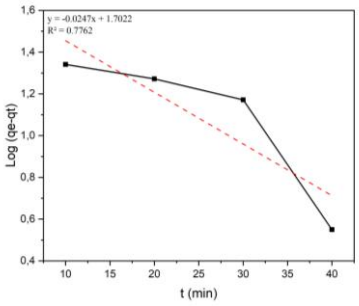


(a)

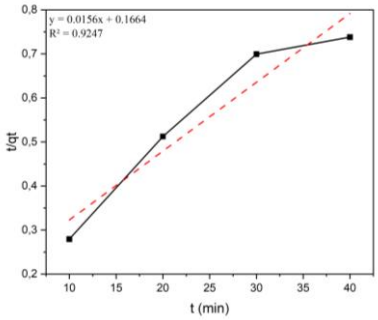


(b)

**Figure 7.** Adsorption models of RBBR onto nitrogen–doped carbon: (a) Pseudo–first–order and (b) pseudo–second–order.

The combined applicability of the pseudo–second–order kinetic model and the Freundlich isotherm suggests that RBBR molecules are not only adsorbed on the external surface but also penetrate into the pore structure of the aerogel. There, that interact with a variety of nitrogen–containing functional groups distributed throughout the adsorbent matrix. This interaction supports a chemisorption–driven multilayer adsorp–tion mechanism, facilitated by the high surface area, porous architecture, and the presence of heteroatoms such as pyridinic N, which act as active adsorption sites.

### 3.5. Adsorption Mechanism

We ilustrated that the mechanisms that control the adsorption of RBBR on the multilayer nitrogen-doped carbon at a solution pH of 6.0, based on prior publications and the aforementioned results (Figure 8), include electrostatic interactions between the negatively charged sulfonate groups ($–SO_3^-$) of RBBR and the protonate

and the protonated pyridinic N on the adsorbent surface (Figure 9).

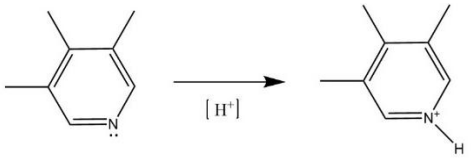


**Figure 8.** Protonation of the pyridinic N group under acidic conditions.

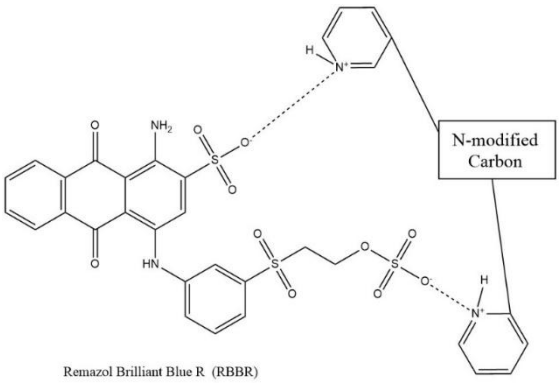


**Figure 9.** Ilustrated mechanism for RBBR dye adsorption onto nitrogen–doped carbon.

This mechanism is supported by adsorption efficiency for RBBR remains high and stable within the pH range of 4–7, attributed to the protonation of surface amine groups ($–NH_2 \rightarrow –NH_3^+$), which enhances their affinity for the sulfonate anions [32]. Similarly, identified pH 6 as the optimal condition for RBBR adsorption, noting that increased proton concentration at lower pH levels enhances the electrostatic attraction between protonated nitrogen sites and the dissociated $–SO_3^-$ groups of the dye [33] .

The sulfonate groups of RBBR exhibit a very low pKa value (<1), implying that they remain fully dissociated as Dye–$SO_3^-$ across a wide pH range above 1 [34]. This is particularly relevant to nitrogen–doped carbons that pyridinic N can be protonated under acidic conditions, contributing to the formation of localized positive charges ($–NH^+$) on the adsorbent surface [35].

### 3.6. Applications on Batik Waste

Nitrogen–modified carbon aerogel was used as an adsorbent to treat double–diluted real wastewater. The adsorption process was conducted at pH 6 for a duration of 60 min. The following data were obtained as presented in Table 3.

**Table 3.** Adsorption performance parameters of nitrogen–doped carbon aerogel for RBBR removal from batik wastewater.

| Parameter | Unit | Result |
|---|---|---|
| Initial concentration | mg/L | 782.42 |
| Concentration adsorbed | mg/L | 485.32 |
| Removal efficiency | % | 62.03 |
| Adsorption capacity | mg/g | 970.65 |

Based on Table 3, adsorbent testing on real batik waste samples evaluated effectiveness in more complex environments. Initial waste concentration of 782.419 mg/L was reduced to 297.097 mg/L, resulting in 62.028% removal efficiency. A significant finding was high adsorption capacity of 970.65 mg/g. This high capacity indicates nitrogen-modified carbon aerogel has strong affinity for RBBR, even in the presence of other impurities in real waste matrices. Although removal efficiency was not 100%, performance is highly promising for batik industrial wastewater treatment. This performance is also better than other adsorbents based on carbon doped N derived from raw materials microcrystal–line cellulose, NaOH, KOH, and urea as shown in Table 4.

**Table 4.** Adsorption performance parameters of nitrogen-doped carbon aerogel for RBBR compared with another adsorbent.

| Adsor–bent | Raw material | Adsorp–tion capacity | Ref. |
|---|---|---|---|
| Activated carbon with N-doped | microcrystal–line cellulose, NaOH, KOH, and urea. | 653.19 mg/g | [6] |
| N-doped Carbon | PEFB with 49% cellulose, Ammonia, NaOH, and urea | 970.65 mg/g | This work |

## 4. CONCLUSION

Nitrogren doped carbon adsorbent that supports environmental sustainability has been successful from the waste of palm empty fruit bunches (PEFB), urea fertilizer, and ammonia. Characterization by XRD, FTIR, and SEM–EDS confirmed the formation of amorphous carbon with pyridinic N functionalities, enhancing surface basicity and adsorption potential. The material proved highly effective for RBBR removal, with optimal performance achieved at 50 minutes contact time and 100 mg/L initial concentration. The adsorption mechanism followed Freundlich isotherm and pseudo–second–order kinetics, indicating a multilayer chemisorption process driven by electrostatic interactions. This work confirms that PEFB–derived aerogel is an efficient, sustainable adsorbent for anionic dyes, offering a viable strategy for valorizing agricultural waste.

## ACKNOWLEDGMENT

This work was supported by State Polytechnic of Malang through Applied Research Innovation Fund Research Grant (SP DIPA–139.03.2.693474/2025).

## REFERENCES

1. M. Ejder-Korucu, A. Gürses, Ç. Doğar, S.K. Sharma, M. Açıkyıldız, Removal of Organic Dyes from Industrial Effluents: An Overview of Physical and Biotechnological Applications, in: S.K. Sharma (Ed.), Green Chemistry for Dyes Removal from Waste Water: Research Trends and Applications, Wiley, 2015: pp. 1–34.
2. M.M. El-Zawahry, F. Abdelghaffar, R.A. Abdelghaffar, A.G. Hassabo, Equilibrium and kinetic models on the adsorption of Reactive Black 5 from aqueous solution using Eichhornia crassipes/chitosan composite, Carbohydr. Polym. 136 (2016) 507–515.
3. Y.-R. Zhang, P. Su, J. Huang, Q.-R. Wang, B.-X. Zhao, A magnetic nanomaterial modified with poly-lysine for efficient removal of anionic dyes from water, Chemical Engineering Journal 262 (2015) 313–318.
4. M.C. Arya, P.S. Bafila, D. Mishra, K. Negi, R. Kumar, A. Bughani, Adsorptive removal of Remazol Brilliant Blue R dye from its aqueous solution by activated charcoal of *Thuja orientalis* leaves: an eco-friendly approach, SN Appl. Sci. 2 (2020) 265.
5. J.M. Divya, K. Palak, P. Vairavel, Optimization, kinetics, equilibrium isotherms, and thermodynamics studies of Coomassie violet dye adsorption using Azadirachta indica (neem) leaf adsorbent, Desalination Water Treat. 190 (2020) 353–382.
6. H. Zhang, L. Xing, H. Liang, J. Ren, W. Ding, Q. Wang, Z. Geng, C. Xu, Efficient removal of Remazol Brilliant Blue R from water by a cellulose-based activated carbon, Int. J. Biol. Macromol. 207 (2022) 254–262.
7. P. Pourhakkak, M. Taghizadeh, A. Taghizadeh, M. Ghaedi, Adsorption: Fundamental processes and applications, Interface Sci. Technol 33 (2021) 71–210.

8. M. Salzano de Luna, F. Greco, R. Pastore, G. Mensitieri, G. Filippone, P. Aprea, D. Mallamace, F. Mallamace, S.-H. Chen, Tailoring Chitosan/LTA Zeolite Hybrid Aerogels for Anionic and Cationic Dye Adsorption, Int. J. Mol. Sci. 22 (2021) 5535.
9. S. Dutta, B. Gupta, S.K. Srivastava, A.K. Gupta, Recent advances on the removal of dyes from wastewater using various adsorbents: a critical review, Mater. Adv. 2 (2021) 4497–4531.
10. C. Patra, T. Shahnaz, S. Subbiah, S. Narayanasamy, Comparative assessment of raw and acid-activated preparations of novel *Pongamia pinnata* shells for adsorption of hexavalent chromium from simulated wastewater, Environmental Science and Pollution Research 27 (2020) 14836–14851.
11. A.A. Yakout, M.A. Shaker, K.Z. Elwakeel, W. Alshitari, Lauryl sulfate@magnetic graphene oxide nanosorbent for fast methylene blue recovery from aqueous solutions, J. Dispers. Sci. Technol. 40 (2019) 707–715.
12. Badan Pusat Statistik, Produksi Tanaman Perkebunan. Badan Pusat Statistik, Https://Www.Bps.Go.Id/Id/Statistics-Table/2/MTMyIzI=/Undefined (2023).
13. L. Agustina, U. Udiantoro, A. Halim, Karakteristik Serat Tandan Kosong Kelapa Sawit (TKKS) dengan Perlakuan Perebusan dan Pengukusan, Zira'ah 41 (2016) 97–102.
14. M.A. Elias, T. Hadibarata, P. Sathishkumar, Modified oil palm industry solid waste as a potential adsorbent for lead removal, Environmental Chemistry and Ecotoxicology 3 (2021) 1–7.
15. S. Susanto, T. Nurtono, W. Widiyastuti, M.-H. Yeh, H. Setyawan, Controlling N-Doping Nature at Carbon Aerogels from Biomass for Enhanced Oxygen Reduction in Seawater Batteries, ACS Omega 9 (2024) 13994–14004.
16. A.D. French, Idealized powder diffraction patterns for cellulose polymorphs, Cellulose 21 (2014) 885–896.
17. M. Fauziyah, W. Widiyastuti, H. Setyawan, Nitrogen-Doped Carbon Aerogels Prepared by Direct Pyrolysis of Cellulose Aerogels Derived from Coir Fibers Using an Ammonia–Urea System and Their Electrocatalytic Performance toward the Oxygen Reduction Reaction, Ind. Eng. Chem. Res. 59 (2020) 21371–21382.
18. M. Fauziyah, W. Widiyastuti, R. Balgis, H. Setyawan, Production of cellulose aerogels from coir fibers via an alkali–urea method for sorption applications, Cellulose 26 (2019) 9583–9598.
19. X. Liu, Organic Chemistry I, 1st ed., Libre Texts, California, 2025.
20. Y. Zhang, F. Wang, H. Zhu, L. Zhou, X. Zheng, X. Li, Z. Chen, Y. Wang, D. Zhang, D. Pan, Preparation of nitrogen-doped biomass-derived carbon nanofibers/graphene aerogel as a binder-free electrode for high performance supercapacitors, Appl. Surf. Sci. 426 (2017) 99–106.
21. M.F.M. Yusop, M.A. Ahmad, N.A. Rosli, F.N. Gonawan, S.J. Abdullah, Scavenging malachite green dye from aqueous solution using durian peel based activated carbon, Malaysian Journal of Fundamental and Applied Sciences 17 (2021) 95–103.
22. H.T. Hii, Adsorption Isotherm and Kinetic Models for Removal of Methyl Orange and Remazol Brilliant Blue R by Coconut Shell Activated Carbon, Tropical Aquatic and Soil Pollution 1 (2021) 1–10.
23. D. Hermanto, P.J. Prihatini, N.Y. Apriani, L. Kurniawati, M. Murniati, S. Hamdiani, N. Ismillayli, S.R. Kamali, Facile Synthesis of Activated Carbon/Alginate/Chitosan Composite Beads as Remazol Brilliant Blue R Adsorbent, Indonesian Physical Review 7 (2024) 480–495.

24. M.A.K. Purnaningtyas, S. Sudiono, D. Siswanta, Synthesis of Activated Carbon/Chitosan/Alginate Beads Powder as an Adsorbent for Methylene Blue and Methyl Violet 2B Dyes, Indonesian Journal of Chemistry 20 (2020) 1119–1130.
25. A.T. Kocer, B. Inan, D. Ozcimen, Adsorption of Remazol Brilliant Blue R by Raw and Carbonized Macroalgal Wastes, Environmental Research and Technology 1 (2018) 40–46.
26. V. Agarwal, H. Metiu, Rates of adsorption and desorption: Entropic contributions and errors due to mean-field approximations, J. Chem. Phys. 150 (2019) 184702.
27. S. Rangabhashiyam, N. Anu, M.S. Giri Nandagopal, N. Selvaraju, Relevance of isotherm models in biosorption of pollutants by agricultural byproducts, J. Environ. Chem. Eng. 2 (2014) 398–414.
28. H. Haryono, A.R. Noviyanti, E.E. Ernawati, Sintesis, Karakterisasi, dan Uji Adsorpsi Komposit Silika/Karbon dari Limbah Sekam Padi sebagai Adsorben Tembaga (II), Jurnal Teknologi Lingkungan 24 (2023) 58–66.
29. D. Setyorini, A. Arninda, A.Q. Syafaatullah, R. Panjaitan, Penentuan Konstanta Isoterm Freundlich dan Kinetika Adsorpsi Karbon Aktif Terhadap Asam Asetat, Eksergi 20 (2023) 149–155.
30. M.M. Nurfarhana, N. Asikin-Mijan, S.F.M. Yusoff, G. Abdulkreem-Alsultan, M.A.R. Othman, S. Kawi, Comparative Study of Adsorption Isotherms on Synthesis of Nitrogen-Doped Porous Carbon by Sodium Amide Activation from Natural Rubber for $CO_2$ Capture, SSRN (2024).
31. C. Meghana, B. Juhi, N. Rampal, P. Vairavel, Isotherm, kinetics, process optimization and thermodynamics studies for removal of Congo red dye from aqueous solutions using Nelumbo nucifera (lotus) leaf adsorbent, Desalination Water Treat. 207 (2020) 373–397.
32. P.M. Nandanwar, D. Saravanan, P. Bakshe, R.M. Jugade, Chitosan entrapped microporous activated carbon composite as a supersorbent for remazol brilliant blue R, Mater. Adv. 3 (2022) 5488–5496.
33. N. Hu, J. Yu, L. Hou, C. Shi, K. Li, F. Hang, C. Xie, Amine-functionalized MOF-derived carbon materials for efficient removal of Congo red dye from aqueous solutions: simulation and adsorption studies, RSC Adv. 13 (2022) 1–13.
34. Y. Zhao, Y. Song, R. Li, F. Lu, Y. Yang, Q. Huang, D. Deng, M. Wu, Y. Li, Enhanced Reactive Brilliant Blue Removal Using Chitosan–Biochar Hydrogel Beads, Molecules 28 (2023) 6137.
35. K. Ide, M. Kunimoto, K. Miyoshi, K. Takano, K. Matsuoka, T. Homma, Surface pH Effects on Catalytic Behavior of Pyridinic Nitrogen on Nitrogen-doped Carbon Nanotube in $CO_2$ Electrochemical Reduction, Electrochemistry 91 (2023) 027003.